



# The effect of topology on the quasi-static and dynamic behaviour of SLM AlSi10Mg lattice structures

Tobias Maconachie<sup>1,2</sup> · Martin Leary<sup>1,2</sup> · Phuong Tran<sup>1</sup> · Jonathan Harris<sup>3</sup> · Qiang Liu<sup>4</sup> · Guoxing Lu<sup>5</sup> · Dong Ruan<sup>5</sup> · Omar Faruque<sup>4</sup> · Milan Brandt<sup>1</sup>

Received: 12 March 2021 / Accepted: 10 October 2021 / Published online: 22 October 2021  
© The Author(s), under exclusive licence to Springer-Verlag London Ltd., part of Springer Nature 2021

## Abstract

Additive manufacturing (AM) techniques such as selective laser melting (SLM) enable the fabrication of complex metallic lattice structures. By tuning geometric and topological parameters, these structures can be manufactured to exhibit a range of useful properties, including excellent strength-to-weight ratios and energy absorption capabilities. While the effects of these parameters on various aspects of AM lattice performance have been previously studied, such as the effects of manufacturability, material selection and geometric parameters on the quasi-static performance of AM lattice structures, the effect of topology on the dynamic behaviour of SLM AlSi10Mg lattice structures remains relatively unexplored. Lattice structure specimens with five different topologies were manufactured using SLM AlSi10Mg and tested under quasi-static and dynamic loading conditions. The tested topologies were body-centred cubic with (BCCZ) and without (BCC) z-struts; face-centred cubic with (FCCZ) and without (FCC) z-struts; and body and face-centred cubic with z-struts (FBCCZ). A numerical model was developed to investigate failure modes and collapse mechanisms. Specimens were found to fail by the emergence of diagonal shear planes, and the orientation of which was dependent on topology, due to the uneven concentration of stress in struts across the structure. No significant rate sensitivity was identified for any of the tested topologies in the range of tested strain rates. The FCCZ topology was demonstrated to provide the greatest efficiency in terms of both strength-to-weight and stiffness-to-weight ratios. These results assist in the characterisation of the dynamic behaviour of SLM AlSi10Mg lattice structures and contribute to their further commercialisation.

**Keywords** SLM · Lattice structures · Dynamic behaviour · Additive manufacture · AlSi10Mg · Mechanical properties

## 1 Introduction

Additive manufacturing (AM) methods, such as selective laser melting (SLM), enable the efficient fabrication of complex and intricate structures that cannot feasibly be obtained by conventional manufacturing methods [1], including lattice structures. Lattice structures are a form of cellular structure that are differentiated from other cellular structures such as metallic foams by the ordered arrangement of their constituent cells [2]. The usefulness of cellular structures has been understood for hundreds of years [3], but with the increasing development of AM, metallic lattice structures have recently received much research attention due to their potential for biomedical [4], aerospace [5] and automotive [6] applications. Lattice structures may be considered meta-materials with properties and behaviours that are distinct, though related to those of their parent material [7]. These properties are dictated

---

✉ Tobias Maconachie  
tobias.maconachie@rmit.edu.au

Martin Leary  
martin.leary@rmit.edu.au

- <sup>1</sup> RMIT Centre for Additive Manufacture, RMIT University, Melbourne, Australia
- <sup>2</sup> ARC Training Centre for Lightweight Automotive Structures (ATLAS), Melbourne, Australia
- <sup>3</sup> nTopology, New York, NY, USA
- <sup>4</sup> Ford Motor Company, Research Innovation Centre (RIC), Dearborn, MI, USA
- <sup>5</sup> Swinburne University of Technology, Melbourne, Australia

by the geometry (size and shape of the structure and its structural elements) and topology (the arrangement and connectivity of structural elements) [8].

Many studies have been conducted on AM lattice structures [9], and it has been found that by tuning lattice geometry and topology, lattice structures can be manufactured to achieve a broad range of properties [10] that cannot be achieved by their parent bulk material [11], including thermal [12], acoustic [13] and mechanical properties [14]. Due to their potential for a range of applications and high commercial value, various studies have sought to characterise the quasi-static mechanical properties of lattice structures, including:

- Yan et al. [15] fabricated stainless steel lattice structures with gyroid unit cells to evaluate their manufacturability and performance. They found that structures with 2–8-mm unit cells could be manufactured without the need for support structures and with good conformity to the intended geometry, and that decreasing unit cell size increased yield strength and modulus.
  - Leary et al. [16] sought to define the manufacturability of particular strut-based topologies and characterise the mechanical performance of lattice structures fabricated in AlSi12Mg using SLM. Lower limits of manufacturability in terms of strut diameter and inclination angle were identified, and the general behaviour of different unit cell topologies was characterised.
  - Leary et al. [8] also investigated the mechanical response, deformation characteristics and failure modes of SLM Inconel 625 lattice structures. The ductility of the material enabled unique insight into transitions between bending and stretch-dominated behaviours for certain cell topologies.
  - Köhnen et al. [17] studied stainless steel lattice structures with two different topologies they referred to as “f2cc,z” and “hollow spherical” under tensile, compressive and cyclical loads. The f2cc,z specimens were found to deform in a stretch-dominated manner, whereas the hollow spherical specimens displayed bending-dominated deformation behaviour, demonstrating the effects of lattice unit cell topology on the plastic behaviour of lattice structures. Specimen geometry was also found to affect the quality of manufacturing outcomes and fatigue performance.
- Although dynamic performance is important for many applications of AM lattice structures, such as fatigue loading of medical implants [18], there is limited data available on their dynamic behaviour. A limited number of studies have sought to define the dynamic behaviour of metallic cellular structures, including:
- Harris et al. [19] investigated the dynamic compressive performance of stainless steel cellular structures manufactured by selective laser melting (SLM). Hybrid cellular structures were fabricated by increasing the porosity of honeycomb structures by replacing walls with lattice struts, which were then dynamically tested using a split-Hopkinson pressure bar apparatus at strain rates between  $5 \times 10^3$  and  $15 \times 10^3 \text{ s}^{-1}$ . Lattice specimens exhibited increased strength at greater strain rates, which was attributed to both the stabilising effect of lateral inertia and wave propagation effects, with wave propagation only occurring above  $10^4 \text{ s}^{-1}$ .
  - Smith et al. [20] fabricated stainless steel lattice structures with BCC and BCCZ topologies using SLM. Specimens were tested at quasi-static strain rates followed by blast tests at strain rates between 210 and  $1710 \text{ s}^{-1}$ . Under quasi-static conditions, BCC specimens failed progressively, whereas the collapse of BCCZ specimens was buckling-dominated. Specimen blast response was found to have a linear dependence on the applied impulse due to the strain rate sensitivity of the material, and collapse modes were found to be similar between quasi-static and blast specimens.
  - McKown et al. [21] tested stainless steel lattice structures with BCC and BCCZ unit cells under quasi-static and dynamic compressive loads at up to  $150 \text{ s}^{-1}$ , followed by blast tests at 450 to  $1815 \text{ s}^{-1}$ . Yield stress was found to be moderately sensitive to strain rate, with a 20% increase over the tested range, due to the rate sensitivity of the parent material and very high strain rates. However, microinertia effects were negligible due to the absence of lateral reinforcement in the tested topologies. Failure modes were found to be similar between quasi-static and blast tests.
  - Tancogne-Dejean et al. [22] conducted numerical, quasi-static, and dynamic tests on 316L stainless steel lattice structures with octet-truss unit cell topology. Dynamic testing was performed using a split-Hopkinson pressure bar setup with an average strain rate of approximately  $1000 \text{ s}^{-1}$ . Lattice specimen strength was found to be significantly dependent on strain rate, though the observed rate sensitivity was close to that of the parent material, suggesting this sensitivity was related to material properties rather than structural phenomena.
  - Ruan et al. [23] studied the compressive behaviour of closed-cell aluminium foams over strain rates ranging from  $10^{-3}$  to  $101 \text{ s}^{-1}$  with relative densities between 5 and 20%. Plateau stress was found to be independent of strain rate, and instead related to relative density by a positive power relationship. Specimen failure did not occur uniformly, but in bands, with each subsequent band failing once the previous band has completely crushed.

However, these studies have focused on small selections of unit cell topologies. In this paper, we aim to test a wide range of lattice topologies to elucidate the influence of strut arrangement and connectivity on the dynamic response of SLM AlSi10Mg lattice structures.

The mechanical performance of cellular structures, including lattice structures, can be generally categorised as either bending-dominated or stretch-dominated [24]. Stretch-dominated structures are characterised by an initial high peak stress followed by a lower plateau stress, whereas bending-dominated structures have a lower initial stiffness followed by a relatively constant plateau stress. Due to these behaviours, stretch-dominated structures are generally stiffer and stronger than bending-dominated structures, whereas bending-dominated structures are more compliant and have a more consistent stress–strain response [25].

The Maxwell criterion [26] provides a means of predicting whether a lattice structure will behave in a bending-dominated or stretch-dominated manner [8] based on the number of struts ( $s$ ) and nodes ( $n$ ) of a lattice unit cell for a given dimensionality (Eq. 1 and Eq. 2) [27]. If  $M < 0$ , the structure is considered *under-stiff*, meaning there are insufficient struts to equilibrate the bending moments at nodes, inducing bending stresses within struts, and resulting in bending-dominated behaviour, whereas if  $M = 0$ , the structure is considered *just-stiff*, or if  $M > 0$ , it is considered *over-stiff*. In these cases, an adequate number of struts are present to equilibrate bending moments at nodes, meaning struts only experience axial stresses, resulting in stretch-dominated behaviour [28].

$$M = s - 2n + 3(2D \text{ truss}) \quad (1)$$

$$M = s - 3n + 6(3D \text{ truss}) \quad (2)$$

However, the Maxwell criterion is understood to be a necessary but insufficient condition for stretch-dominated behaviour [26], and previous studies of lattice structures have found certain lattice topologies to be capable of behaving in a stretch-dominated manner, despite being under or just-stiff according to the Maxwell criterion [8, 16, 29, 30]. In this study, lattice structure specimens with five different topologies are tested under quasi-static and dynamic loads to better understand the topological and dynamic effects on their mechanical behaviour.

In this work, lattice specimens with BCC, BCCZ, FCC, FCCZ, and FBCCZ topologies and all geometric parameters kept constant were tested under quasi-static and dynamic loading conditions, with comparison to numerical models of lattice specimens to identify topological and dynamic effects on the compressive mechanical behaviour of SLM AlSi10Mg lattice structures. The results of quasi-static and dynamic testing are discussed, with reference to stress–strain behaviour and qualitative analysis of photography acquired during testing and compared with results of the numerical

model. These findings assist in the comprehensive characterisation of lattice structures in both quasi-static and dynamic loading regimes and facilitate the further commercialisation of AM lattice structures.

## 2 Specimen design and manufacture

Certain technical limitations exist regarding the manufacturability of components using SLM and aluminium powder. For example, the relatively high absorptivity of aluminium powder due to internal reflections [31] combined with its relatively high diffusivity means greater power is required for SLM than other metals, such as titanium [16]. AlSi10Mg components produced by SLM are also prone to anisotropic mechanical properties [32]. As a result, although SLM enables the fabrication of complex, intricate structures [33], it is also subject to manufacturability limitations. To ensure feasibility for this study, specimen designs were based on the manufacturability findings of a previous study [16].

### 2.1 Topology and geometry

To investigate the interaction between topological and dynamic effects on the mechanical behaviour of AlSi10Mg lattice structures, specimens were designed with five different unit cell topologies, referred to as BCC (body-centred cubic), BCCZ (body-centred cubic with z-struts), FCC (face-centred cubic), FCCZ (face-centred cubic with z-struts) and FBCCZ (face and body-centred cubic with z-struts). The topological details and relative densities of the CAD models unit cells considered here are presented in Table 1. All specimens were designed with  $5 \times 7.5$  mm cubic cells in each orthogonal direction with 1-mm diameter struts. An example of the CAD geometry of a BCC specimen, including strut diameter and cell size, is presented in Fig. 1.






### 2.2 Manufacture of specimens

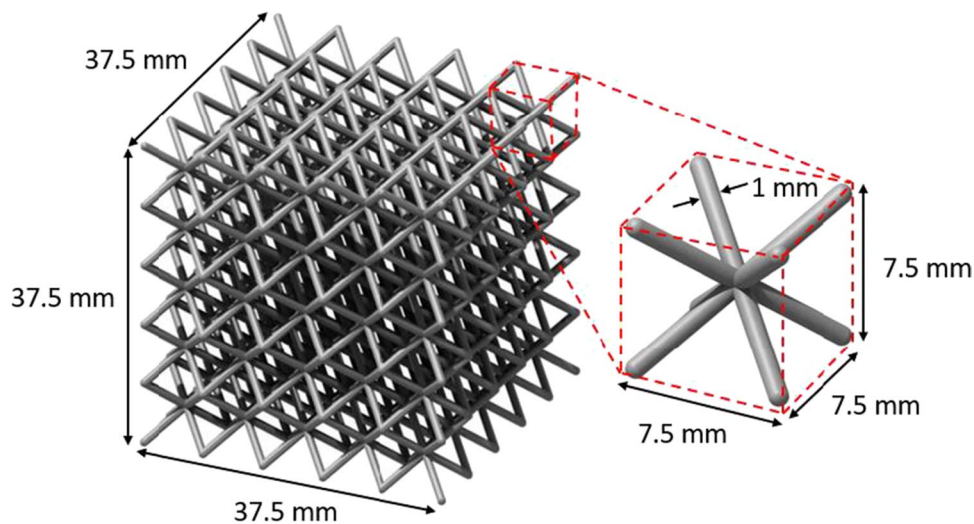
Lattice specimens were fabricated using a SLM Solutions 400 W dual laser powder bed SLM 500. The processing parameters used are presented in Table 2. The chemical composition of the AlSi10Mg powder used is presented in Table 3, and the powder particle size distribution is presented in Fig. 2.

## 3 Mechanical testing

To enable comparison between quasi-static and dynamic behaviour, as-manufactured lattice specimens were tested under both quasi-static and dynamic loadings. Strain was calculated based on crosshead displacement and specimen height (37.5 mm), and compressive stress was calculated by

**Table 1** Lattice specimen unit cell topological details

Topology	Body-centred cubic (BCC)	Body-centred cubic with z-struts (BCCZ)	Face-centred cubic (FCC)	Face-centred cubic with z-struts (FCCZ)	Face and body-centred cubic with z-struts (FBCCZ)
Image					
Struts ( $s$ )	8	12	16	20	28
Nodes ( $n$ )	9	9	12	12	13
Maxwell number ( $M$ )	-13	-9	-14	-10	-5
Struts oriented in load direction	No	Yes	No	Yes	Yes
Relative density of CAD model (%)	8.5	9.6	6.99	8.01	15.58

**Fig. 1** CAD representation of BCC lattice specimen, including definition of geometric parameters**Table 2** SLM processing parameters

Parameter	Value
Layer thickness ( $\mu\text{m}$ )	30
Laser power (watts)	370
Laser velocity (mm/s)	1335
Hatch spacing ( $\mu\text{m}$ )	170

dividing the measured load by the nominal cross-sectional area of the specimens ( $37.5^2 \text{ mm}^2$ ).

### 3.1 Quasi-static testing

Two specimens of each topology were tested under quasi-static loading using an MTS Landmark with a 100-kN load cell. Specimens were loaded at  $10^{-3} \text{ s}^{-1}$  (2.25 mm/min). Time-lapse photography with a frequency of four images per minute was used to record all experiments and identify failure modes.

**Table 3** Chemical composition of AlSi10Mg powder (%)

Al	Si	Cu	Fe	Mg	Zn	Cr	Ni	Mn	Ti	Sr	Zr	V	Ag	C	N	O
Balance	10.2	<0.01	0.19	0.34	0.01	0.01	0.01	<0.01	0.01	<0.001	<0.005	0.005	<0.005	<0.005	0.002	0.12

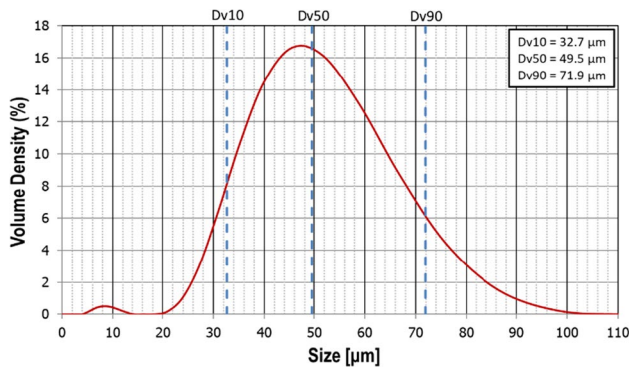


**Fig. 2** Powder particle size distribution acquired by spectrographic analysis

Young’s modulus was identified from the gradient of the linear region of the quasi-static stress–strain curve, yield stress was quantified using the 0.2% strain offset method and ultimate strength was the maximum stress carried by specimens before failure.

Ashby et al. [34] suggest that measuring the Young’s modulus of a cellular structure in the conventional manner—the stress–strain ratio during the linear region of elastic deformation—is unrepresentative of the structure’s functional stiffness, due to local plasticity occurring in the structure at stresses well before yielding. Instead, they recommend that measurement of a cellular structure’s modulus be taken from the slope of the unloading curve. For this reason, the unloading modulus of one specimen of each topology was measured at 1% and 2% strain, as well as the conventional Young’s modulus, as has been performed in previous studies [8].

### 3.2 Dynamic testing

Dynamic testing was performed using an Instron VHS8800 testing machine with a loading capacity of 80 kN. Three specimens of each topology were tested at 5 m/s (corresponding to a strain rate of  $133.33 \text{ s}^{-1}$ ), which was maintained constant during the testing procedure. High-speed photography was used to capture images during testing for identification of associated failure modes.

A meaningful measurement of Young’s modulus, and therefore yield stress, cannot be extracted from a dynamic stress–strain curve in the same manner as a quasi-static test due to the non-uniform deformation associated with

dynamic loading. As a result, dynamic results were analysed in terms of ultimate compressive strength.

### 3.3 Normalised properties

It is understood that the mechanical performance of cellular structures is dependent on their relative densities [24]. The lattice specimens considered in this study were designed with the same geometric parameters (cell size and strut diameter) with the only variation in topology. However, these geometric and topological parameters affect the relative density of a lattice structure and therefore the mechanical performance. To compare normalised properties, specific strength and specific modulus were calculated by dividing specimen properties by their density.

The relative density ( $\rho^*/\rho_s$ ) of each specimen was calculated based on their mass ( $m_s$ ), their nominal volume ( $V_s$ ) and the density of the material ( $\rho_s$ ), which was assumed to be  $2.67 \text{ g/cm}^3$  (Eq. 3).

$$\frac{\rho^*}{\rho_s} = \frac{m_s}{V_s \rho_s} \tag{3}$$

### 3.4 Energy absorption

The energy absorbed during testing per unit volume ( $W_V$ ) and per unit mass ( $W_M$ ), based on the specimen density ( $\rho$ ), were calculated using Eq. 4 and Eq. 5 respectively. Calculations were based on stress ( $\sigma$ ) and strain ( $\epsilon$ ) behaviour, measured between the start of the test and strain at failure ( $\epsilon_f$ ).

$$W_V = \int_0^{\epsilon_f} \sigma d\epsilon \tag{4}$$

$$W_M = \frac{1}{\rho} \int_0^{\epsilon_f} \sigma d\epsilon \tag{5}$$

## 4 Finite element modelling

To investigate collapse behaviour and deformation mechanisms, a finite element (FE) model was developed to replicate the behaviour of the candidate lattice structures (Fig. 3) using the ABAQUS static and dynamic explicit solvers. Lattice struts were represented using 2-node linear beam

elements in space (B31) with circular cross-sections that matched the experimental specimen's topological and geometric parameters (1-mm diameter, 7.5-mm cell size, 5 cells in  $x$ ,  $y$ , and  $z$  directions). Beam elements provide a computationally efficient means of modelling lattice structures [35, 36] and are appropriate to modelling applications including geometric nonlinearity and material plasticity [37], as is the case when modelling lattice structures. However, there are known limitations of modelling lattice structures using beam elements, such as the inability to directly model geometric defects that result from AM fabrication methods [37], and do not account for overlapping volumes at strut intersection [35]. Despite these disadvantages, and due to the exceptional computational efficiency of beam elements [38] compared to alternative continuum elements [39], beam elements have been used to effectively model the compressive behaviour of lattice structures in several previous studies [35–41].

Specimens were crushed between plates represented by rigid elements (R3D4) that moved at a constant prescribed velocity with a unit mass. Quasi-static tests were replicated using the static solver and dynamic tests using the dynamic explicit solver with a strain rate of  $100 \text{ s}^{-1}$ . Mesh density analysis was performed, and a global element size of 10% of cell size (0.75 mm) was found to lead to convergence of results for all topologies.

General contact was set for the whole model, to enable load transfer between the plates and lattice, and to constrain the displacement of struts by contact with each other. Normal behaviour was defined as “hard contact,” and friction between the specimens and the rigid plates was modelled by defining the tangential behaviour as “penalty” with a coefficient of friction of 0.1.

An elastic/plastic material model was defined using parameters identified in a previous study on SLM AlSi10Mg [32]. Elastic parameters were Young's modulus = 68 GPa

and Poisson's ratio = 0.3. Material plasticity was defined using the Johnson–Cook model (Eq. 6). Constitutive relationships between build orientation angle and strain hardening parameters of SLM AlSi10Mg were previously identified, and so different material models were applied depending on the orientation of struts (Table 4), which was found to reduce error between the experimental and FE model results.

$$\sigma = [A + B\epsilon^n][1 + C\ln(\dot{\epsilon}^*)][1 - T^{*m}] \quad (6)$$

where  $\sigma$  = plastic flow stress;  $A$  = material yield strength;  $B$  = strain hardening coefficient;  $\epsilon$  = strain;  $n$  = strain hardening exponent;  $C$  = strain rate sensitivity;  $\dot{\epsilon}^*$  = ratio of given strain rate to the reference strain used to determine strain hardening coefficient and exponent;  $T^*$  = non-dimensional temperature, function of room temperature, the material's melting temperature and reference temperature used to determine strain hardening coefficient and exponent;  $m$  = thermal softening exponent.

The Johnson–Cook model enables the modelling of material strain rate sensitivity. However, previous studies have concluded that SLM AlSi10Mg can be modelled as non-strain rate sensitive in the  $1\text{--}100 \text{ s}^{-1}$  range [32, 42, 43], so no strain rate sensitivity value was prescribed ( $C=0$ ). Temperature was not considered in this study, so temperature parameters were ignored in the material model ( $T=0$ ).

**Table 4** Johnson–Cook plasticity model parameters for vertical and inclined struts [32]

Strut orientation	$A$ (MPa)	$B$ (MPa)	$n$
Vertical	259.6	1,581.59	0.76
Inclined	264.54	1,278.43	0.71

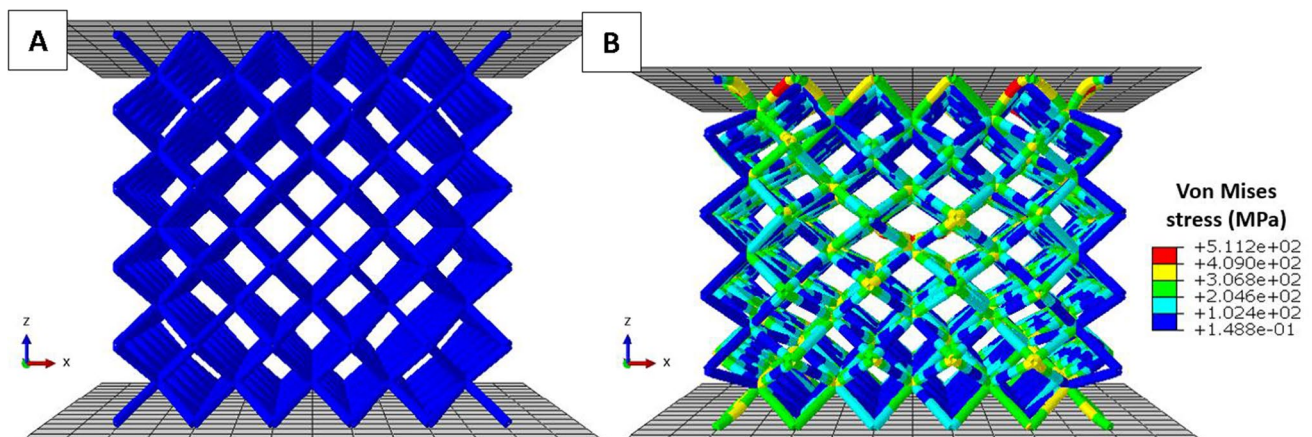


**Fig. 3** Finite element model, including **A** undeformed and **B** deformed state. Lattice specimens are represented using beam elements and crushed between rigid plates

## 5 Results and discussion

To account for the different relative densities of specimens and the effect on mechanical performance, the relative densities of the specimens were identified and are discussed. Quasi-static and dynamic mechanical testing results are compared, and insights provided by the FE model are explored.

### 5.1 Relative density

The average relative densities of as-manufactured specimens for all topologies are compared with the predicted value based on specimen CAD in Fig. 4. As-manufactured relative densities of body-centred topologies (BCC, BCCZ and FBCCZ) were consistently less than those predicted by the CAD, while FCC and FCCZ as-manufactured relative densities were greater than those predicted by the CAD. SLM-manufactured components are prone to shrinkage during manufacture due to the difference in cooling rates between surface and subsurface [44], which may explain the reduced density of as-manufactured body-centred specimens. Unlike the BCC topology, the face-centred topologies (FCC, FCCZ and FBCCZ) share struts between cells. However, for unit cells on the outer surfaces of a lattice structure, the volume of struts that are not shared between unit cells is not accounted for, leading to a greater difference between the CAD relative density and that of the as-manufactured specimens. This difference increases with the number of unit cells, and as specimens had many unit cells on their faces (25 cells per face on six faces) this difference was significant compared to other topologies. As the FBCCZ includes both FCC and BCC struts, the difference between the idealised CAD and as-manufactured relative densities is due to that not accounting for shared struts on the specimen faces is

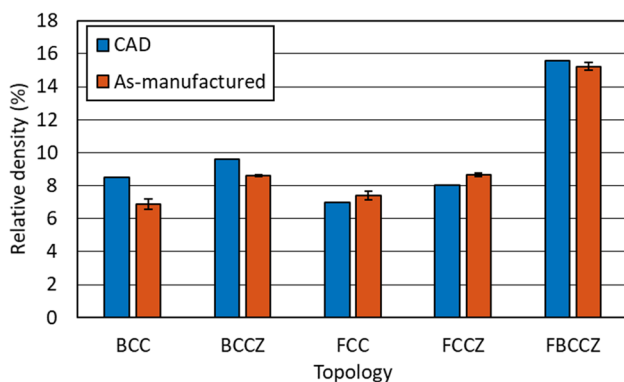


**Fig. 4** Comparison of CAD and average relative densities of as-manufactured specimens for all topologies. Error bars for as-manufactured specimens indicate one standard deviation

offset by the error due to shrinkage of struts, meaning the relative density of as-manufactured FBCCZ specimens was less than that predicted by the CAD.

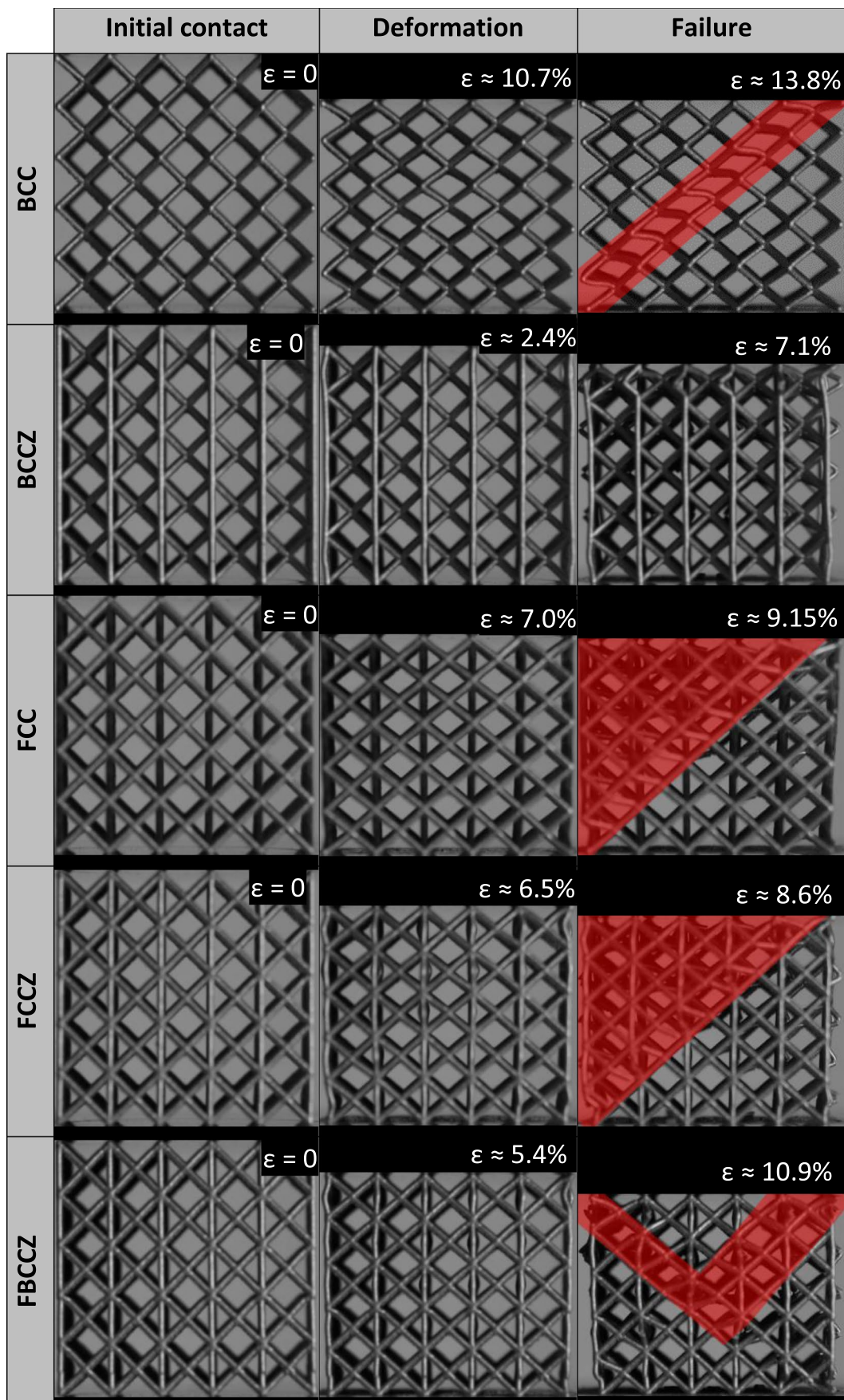
### 5.2 Quasi-static results

Selected images of lattice specimens during quasi-static testing are presented in Fig. 5. When failure occurred, diagonal failure planes emerged (red highlights in Fig. 5) for all topologies. For BCC and BCCZ specimens, the failure plane was diagonal on two of the parallel vertical planes, but horizontal on the perpendicular planes, whereas for FCC and FCCZ specimens, the failure plane was diagonal on all vertical planes (Fig. 6), demonstrating that the orientation of failure planes is dependent on topology. For the specimen with z-struts, deformation was concentrated in the layers in contact with the compression plates, but once the z-struts failed (usually on the upper layer which was in contact with the moving plate) failure planes emerged, with their orientation depending on the presence of BCC or FCC struts. The FBCCZ specimens were not as consistent in their failure mechanism, with no single plane of failure emerging, and failure occurring within random cells through the structure. The FBCCZ specimens were also able to hold together post-failure, unlike the other topologies, due to the significant number of struts present, suggesting a potential greater damage tolerance of this topology.

Stress–strain curves for the tested specimens are presented in Fig. 7A. Specimens with z-strut topologies (BCCZ, FCCZ and FBCCZ) showed greater stiffness and strength than those without, with stress–strain curves that suggest a stretch-dominated response, while both BCC and FCC specimens failed at greater strains than their z-strut counterparts, and behaved in a bending-dominated manner, consistent with previous studies [10, 16]. This suggests that the inclusion of z-struts increases strength and stiffness, though at the cost of reduced compliance.

All specimens behaved in a brittle manner—once the ultimate strength was reached, the specimens catastrophically failed, and experiments were stopped. Unlike the other topologies, FBCCZ specimens failed progressively, as no single failure plane emerged, as shown in Fig. 5. As-manufactured SLM AlSi10Mg has previously been found to be brittle [45–47], and SLM lattice structures with similar geometries made from different materials such as Inconel and Ti6Al4V have been found to be more ductile [8, 30]. This suggests the observed brittle behaviour of the lattice structures is due to the brittleness of the material.

Stress–strain curves normalised by specimen density (specific stress–strain) are presented in Fig. 7B and yield, and ultimate strengths normalised by specimen density (specific strength) are presented in Fig. 7C. Although





◀ **Fig. 5** Photographs of initial contact, deformation and failure of quasi-static specimens during testing. Build direction is upwards and loads are vertical. Red highlights indicate failure planes. The failure plane of the BCCZ specimen occurred on the face not visible to the camera

FBCCZ had the greatest yield and ultimate strengths (Fig. 7A), this is partially due to the greater material presence provided by the extra struts, and when mass is accounted for, FCCZ is the most efficient topology in terms of strength-to-weight ratio. Conversely, although the BCC and BCCZ specimens had greater relative density than the FCC and FCCZ topologies respectively, the superior specific strength of the FCC and FCCZ specimens demonstrates that relative density is not the only contributing factor to lattice mechanical performance, and that topology significantly affects qualitative and quantitative performance.

An example of the Young's modulus, 1% and 2% unloading moduli are provided in Fig. 8A, and these values for all topologies normalised by specimen densities (specific modulus) are compared in Fig. 8B. The Young's modulus of specimen that were and were not unloaded was very similar, though for BCC, BCCZ and FCC specimens the Young's modulus of the unloaded specimens was greater than that without unloading, whereas for the FCCZ and FBCCZ specimens the opposite was observed. This suggests that unloading reduces the Young's modulus of specimens with FCCZ topologies. The unloading moduli were consistently greater than the Young's modulus for all specimens, and the 2% unloading modulus was always greater than the 1% unloading modulus, suggesting stiffness increases with an increase in the strain at which the specimen is unloaded. These findings support Ashby's assertion that unloading modulus is more representative of a structure's stiffness due to the similarity between the unloading moduli and their difference to the Young's modulus.

The effect of the inclusion of z-struts on specific modulus is apparent from Fig. 8B—z-struts significantly increase the modulus of lattice topologies, as seen by the superior modulus of the BCCZ and FCCZ topologies compared to the BCC and FCC topologies, respectively. Comparison of Fig. 7C (specific strength) and Fig. 8B (specific modulus) shows that z-struts more significantly contribute to the stiffness of the lattice than strength, as seen by an increase in specific modulus provided by the inclusion of z-struts, compared to the increase in specific strength.

### 5.3 Dynamic results

High-speed photographs of specimens during dynamic testing are presented in Fig. 9. Specimens failed due to the

emergence of diagonal shear planes, as was observed during quasi-static testing. Greater deformation was observed on the loaded (top) face of the specimens with z-struts (BCCZ, FCCZ and FBCCZ), whereas deformation was more evenly distributed through the specimen for specimens without z-struts (BCC and FCC). Failure occurred at greater strains under dynamic loading compared to the quasi-static results due to the increased rate of deformation.

Specimens behaved in a brittle manner under dynamic loading—once softening occurred the specimens catastrophically failed—consistent with the brittle behaviour observed during quasi-static testing. This suggests that conservative safety factors would be necessary for the implementation of as-manufactured SLM AlSi10Mg lattice structures to keep their maximum operating stresses within the linear region of their stress–strain curve.

Dynamic stress–strain curves for selected specimens of all topologies are compared in Fig. 10A. Similar to the quasi-static stress–strain curves (Fig. 8A), it is shown that the inclusion of z-struts increases the stiffness and strength but reduces the strain at which failure occurred.

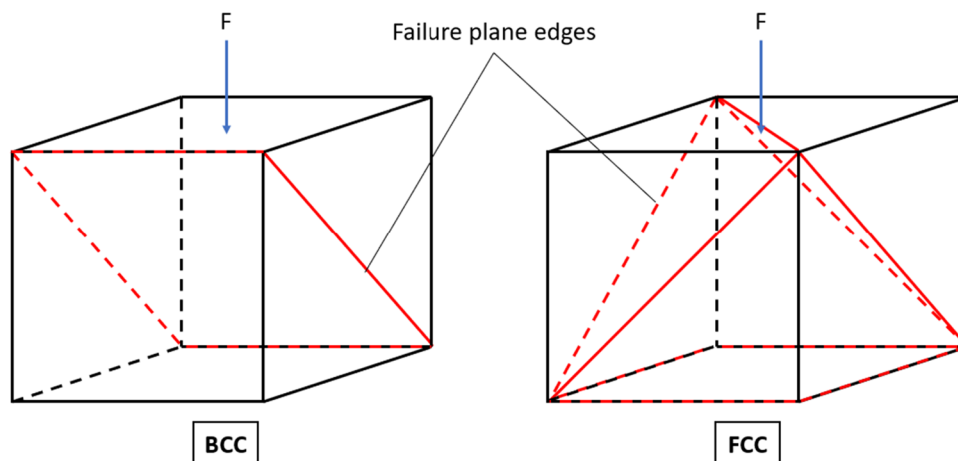
Comparison of dynamic specific ultimate compressive strength between topologies (Fig. 10B) shows that FCCZ is the most efficient topology in terms of strength-to-weight ratio under dynamic loadings as well as quasi-static loading. The results were very consistent, with only minor standard deviations for all topologies.

### 5.4 Comparison of quasi-static and dynamic results

Stress–strain curves of selected quasi-static and dynamic specimens are compared in Fig. 11A. Although the general shape of the curves for a given topology is quite similar, the shallower gradient of the dynamic curves after failure shows that specimens failed over a larger strain compared to quasi-static result, due to the increased strain rate of the dynamic experiments. The peak of the curves generally occurred at greater strain under dynamic loading, which is consistent with the greater strain at failure for dynamically tested specimens, as seen by comparison of the strain in Figs. 5 and 9. This suggests that the general behaviour of all topologies is quite similar between quasi-static and dynamic loading regimes, though the increased rate of the dynamic testing means that the certain phenomena, such as yielding, peak stress and failure, occur at greater strains under increased loading rate.

The scatter plot presented in Fig. 11B shows the specific strength of all specimens over the range of tested strain rates. Although most topologies showed very similar specific strength at both quasi-static and dynamic strain rates, suggesting a lack of rate sensitivity, FCC specimens seemed to show an increase in specific strength in the dynamic rate range, whereas FCCZ showed a drop in specific strength at

**Fig. 6** Schematic representation of failure plane orientation on faces of BCC and FCC specimens with respect to the applied load (F)



the greater strain rate, compared to the quasi-static response. However, when mean strength values are compared, as presented in Fig. 11C, very little difference is observed between the quasi-static results—BCC, FCC and FCCZ had the greatest variation in mean specific strength over the tested strain rates, with a 5%, 4.5% and 4.6% change in specific strength, respectively. BCCZ and FBCCZ were the most consistent across the tested strain rates with only 1.7% and 0.5% differences, respectively. These results suggest that the strength of all topologies is not significantly strain rate sensitive.

## 5.5 Energy absorption

The energy absorbed per unit volume and per unit mass is presented in Fig. 12A and B respectively. The energy absorbed per unit volume ( $W_v$ ) consistently increased with strain rate for all topologies except FCCZ—12% for BCC, 18% for BCCZ, 23% for FCC and 4% for FBCCZ—whereas FCCZ saw a 12% drop in energy absorbed per unit volume. This is due to the decreased ultimate strength of the dynamically tested specimens seen in Fig. 11A, leading to an overall reduction in energy absorption in the dynamic strain rate range. Differences in  $W_v$  between topologies reflect differences in modulus and strength values discussed above, as all specimens had the same nominal volume.

When energy absorption was normalised by specimen density (energy absorbed per unit mass,  $W_M$ , Fig. 12B), FCCZ and FBCCZ topologies were found to significantly outperform the BCC, BCCZ and FCC topologies— $W_M$  for BCC, BCCZ and FCC specimens ranged between 0.65 and 0.86 J/g, whereas that for FCCZ and FBCCZ ranged between 1.4 and 1.6 J/g. The inclusion of z-struts in the BCC topology led to a 12% increase in  $W_M$  in the quasi-static range, and a 23% increase in the dynamic range, suggesting that the z-struts provide more mass-efficient energy absorption capabilities. However, a more significant increase in  $W_M$  was observed due to the inclusion of

z-struts in the FCC topology—a 140% increase in  $W_M$  was observed in the quasi-static range and a 66% increase in the dynamic range. This demonstrates that the inclusion of z-struts has a more significant effect on the FCC topology compared to the BCC topology in terms of energy absorption, and further demonstrates the efficiency of the FCCZ topology, as well as the efficiency of strength- and stiffness-to-weight ratios. FBCCZ specimens had lower  $W_M$  than the FCCZ specimens in the quasi-static range suggesting the presence of both BCC and FCC struts is inefficient, and that impressive energy absorption can be achieved with the FCCZ topology without the need for BCC struts. FBCCZ specimens had the greatest  $W_M$  of all specimens, as they were able to hold together for the greatest strain, as previously discussed, due to the greater presence of material within cells, meaning failure occurred over a greater strain, increasing energy absorption performance.

These results further demonstrate that relative density of a lattice structure's unit cell does not alone dictate its performance, and that topology can be used as a coarse design parameter to radically alter the compressive performance of lattice structures.

Again, all topologies showed an increase in  $W_M$  with increased strain rate except FCCZ, which showed a mean decrease of 11%. This improved energy absorption performance is due to stress-strain phenomena occurring at higher strains during dynamic deformation, as previously discussed. As yielding, peak strength and failure occur at higher strains under dynamic loading, due to increased rate of deformation, more energy is absorbed over that greater strain. This demonstrates that SLM lattice structures may be effectively deployed for energy absorption applications under dynamic loading, as their energy absorption performance is increased with the increased strain rate.

The energy absorption capabilities of the tested lattice structures were hampered by the brittleness of the

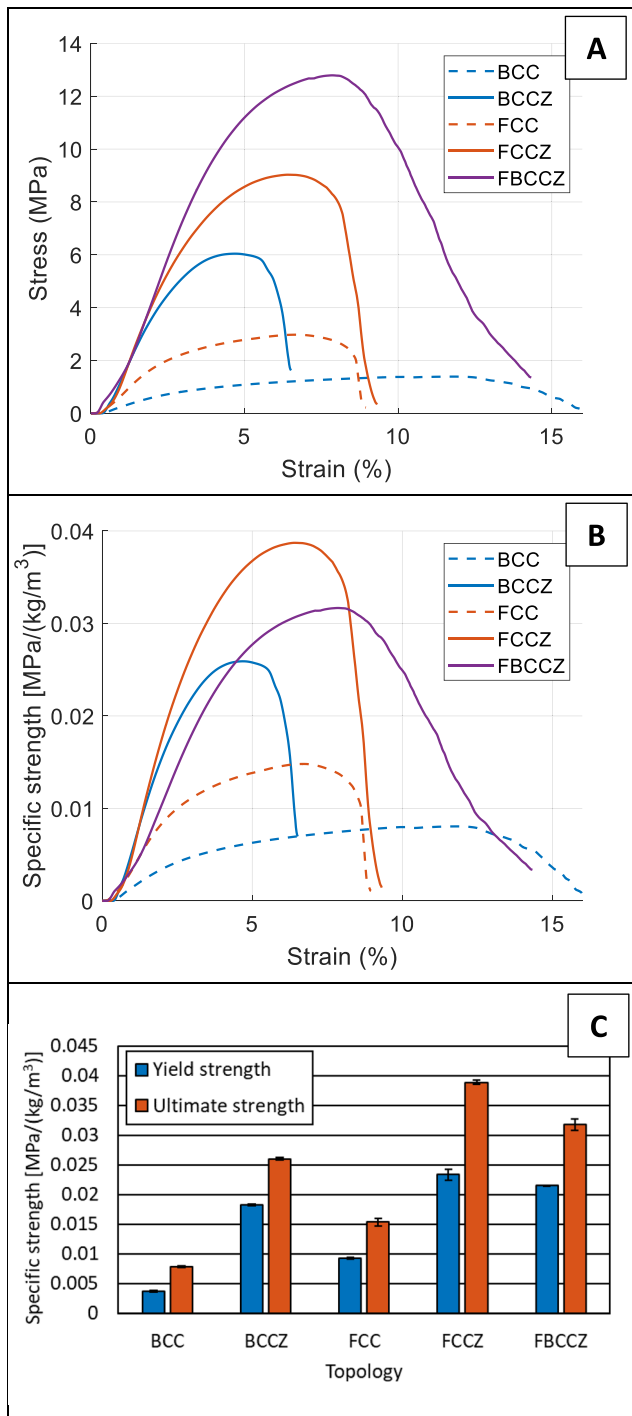


**Fig. 7** Quasi-static results, including **A** stress–strain curves, **B** specific stress–strain curves and **C** specific yield and ultimate strengths of all tested topologies

specimens in their as-manufactured state, as no plateau stress could be achieved before catastrophic failure upon yielding, even for the BCC specimens—the most compliant topology. Although results demonstrate that energy absorption efficiency is dependent on topology, the

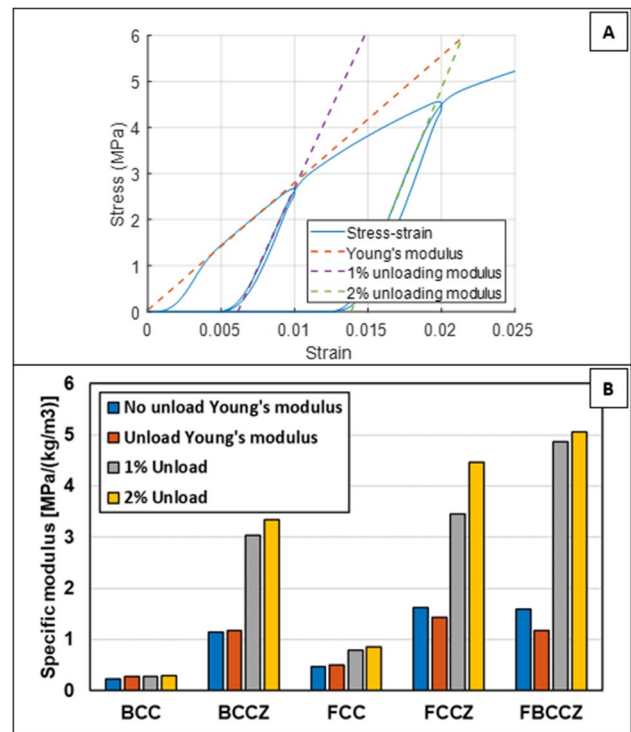
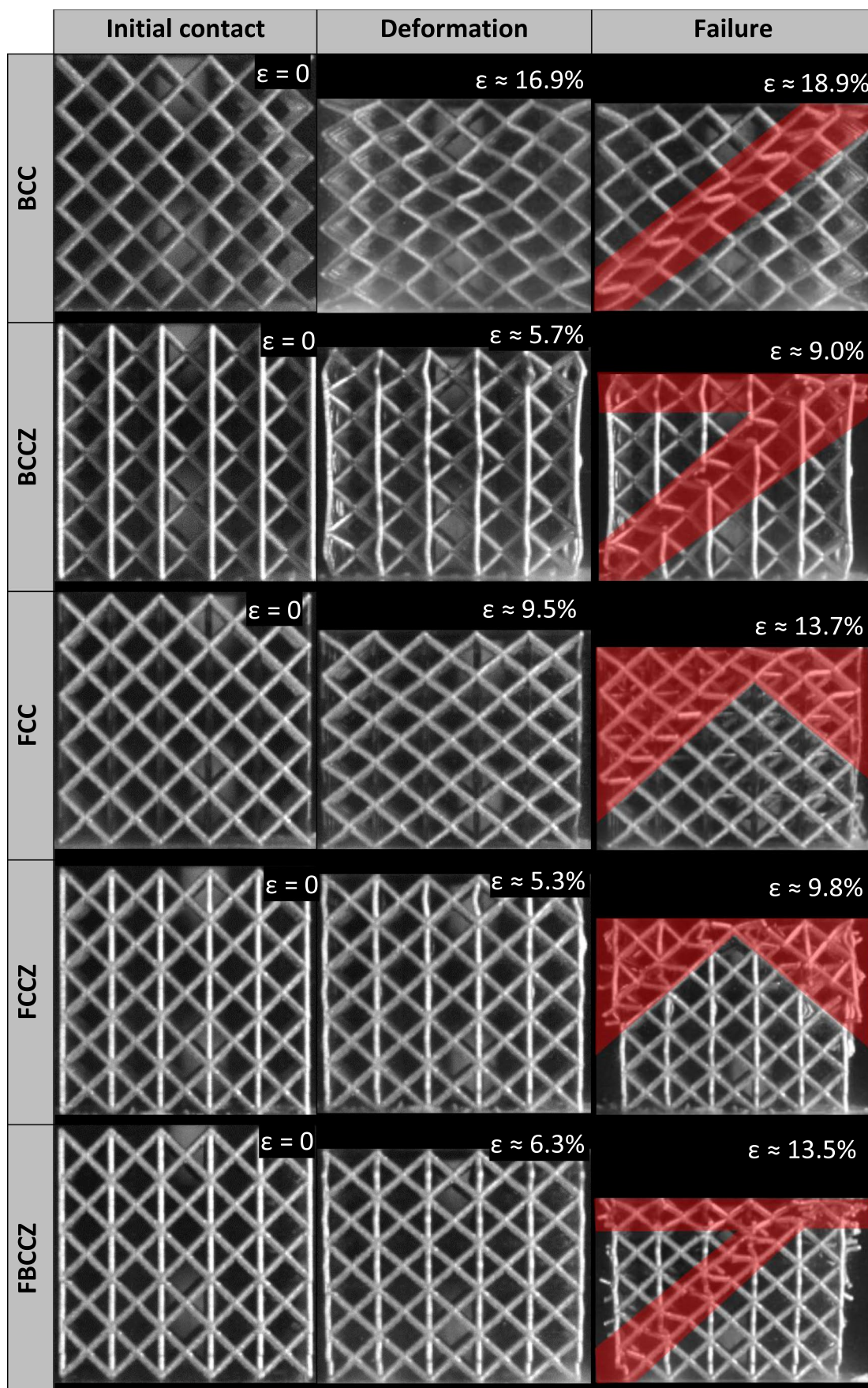


**Fig. 8** **A** Comparison of Young’s modulus, 1% and 2% unloading modulus and **B** specific Young’s modulus of the specimens tested without unloading, and the specific Young’s modulus and 1% and 2% moduli of the specimen tested with unloading

brittleness of the specimens suggests that these particular lattice structures would not be very useful for energy absorption applications in their as-manufactured state, as the continuous deformation observed in the plateau region of compliant cellular structures, which is desirable for energy absorption applications, was absent here. However, the brittleness of SLM AlSi10Mg has been reported previously [48, 49], and to overcome this heat treatments including annealing and hot isostatic pressing (HIP) [50] have been shown to improve ductility at the cost of strength [51] of bulk SLM AlSi10Mg. Furthermore, heat treatments on lattice structures have demonstrated that mechanical performance can be improved due to reduced porosity [52] and even reduce strain rate sensitivity [53]. Although the effect of heat treatment on the performance of SLM AlSi10Mg lattice structures is not within the scope of this study, results from the literature suggest the brittleness of the as-manufactured specimens may be overcome by heat treatment, which would improve their energy absorption performance.

### 5.6 Numerical modelling

Quasi-static and dynamic stress–strain curves extracted from experiments and simulations are compared in Fig. 13, along



◀ **Fig. 9** High-speed photographs of specimens during dynamic testing at initial contact, during deformation, and after failure. Build direction is upwards and loads are vertical. Red highlights indicate failure planes

with specific Young's modulus. It can be seen that although there was a good match between the curves for the lattice structures without z-struts (BCC and FCC), the stiffness of simulations of the structures including z-struts (BCCZ, FCCZ and FBCCZ) was consistently greater than that of the experimental curves. This finding is consistent with previous studies comparing the simulated and experimental behaviours of lattice structures. For example, Luxner et al. [35] found that for lattice structures whose response is highly directionally dependent, as is the case when struts oriented in the build direction are included (z-struts), there is greater error between simulation and experimental curves, as these structures are very sensitive to changes in loading direction. Smith et al. [36] compared simulated and experimental mechanical properties of BCC and BCCZ lattice structures and also found that there was a better match between the stiffness of simulations and experiments of BCC lattice structures compared to BCCZ. These results suggest that the accuracy of numerical modelling of lattice structures is highly dependent on the governing deformation mechanisms [35], and that structures that rely on buckling for failure (stretch-dominated), such as those topologies including z-struts, tend to have greater variation between simulated and experimental results than structures that fail by bending (bending-dominated).

There are both aleatory and epistemic uncertainties associated with experimental testing of AM lattice structures that result in discrepancies between numerical and experimental results. Variation in the intended and as-manufactured geometries is a known limitation of AM technologies [54], including SLM [55], that has been found to significantly affect the performance of AM lattice structures [56]. The relative density results of this study (Sect. 5.1) further demonstrate that the magnitude of these discrepancies is dependent on topology. Inconsistencies in as-manufactured geometries mean identification of precise mechanical properties of individual struts within lattice structures is difficult [39], particularly strut radius along their length [37]. These geometric discrepancies also have implications for the orientation of loads applied to struts, which is known to have a significant effect on buckling performance [57], and is the dominant failure mode for lattice structures with z-struts. Friction between the lattice specimens and compression plates affects the mechanical performance of lattice structures [58], yet it is understood that there is significant variation in the roughness of upward- and downward-facing surfaces of specimens manufactured by SLM [59]. This suggests the friction behaviour on the upper and lower faces of the lattice specimens

could be quite different, yet this effect remains unquantified and difficult to account for in numerical models. The significance of these factors varies depending on topology and means the ability of the numerical model to precisely predict mechanical properties such as stiffness and strength is equally topologically dependent.

While there was quantitative discrepancy between the stress–strain behaviour of simulations and experiments, particularly in terms of the stiffness of specimens with z-struts, the qualitative behaviour matched quite well. The general shape of the stress–strain curves (Fig. 13) of simulations during initial deformation matched well with experimental curves, though discrepancies increased at larger strains due to the absence of a fracture mechanism in the model. The deformation of experimental and simulated lattice specimens is compared in Fig. 14 and is considered to match quite well—the initial buckling of struts and the concentration of deformation in upper and lower layers in contact with compression plates match between simulations and experiments. Stress contours during the early stages of deformation of the numerical model were found to provide significant insight into the causes of macroscopically observed experimental behaviour, particularly with regard to the variations between the tested topologies. The purpose of the numerical model implemented in this study was to provide insight

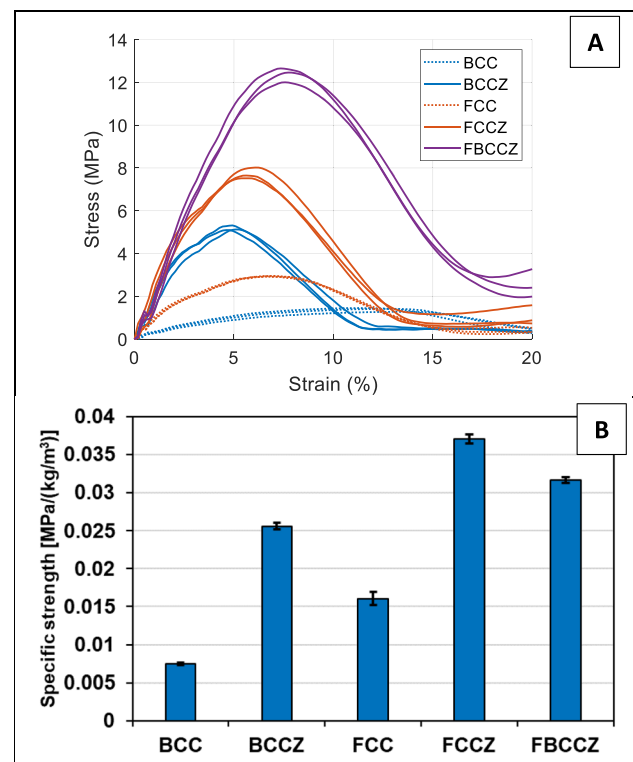


**Fig. 10** Dynamic results, including **A** example stress–strain curves and **B** comparison of mean specific strength of all topologies. Error bars indicate one standard deviation

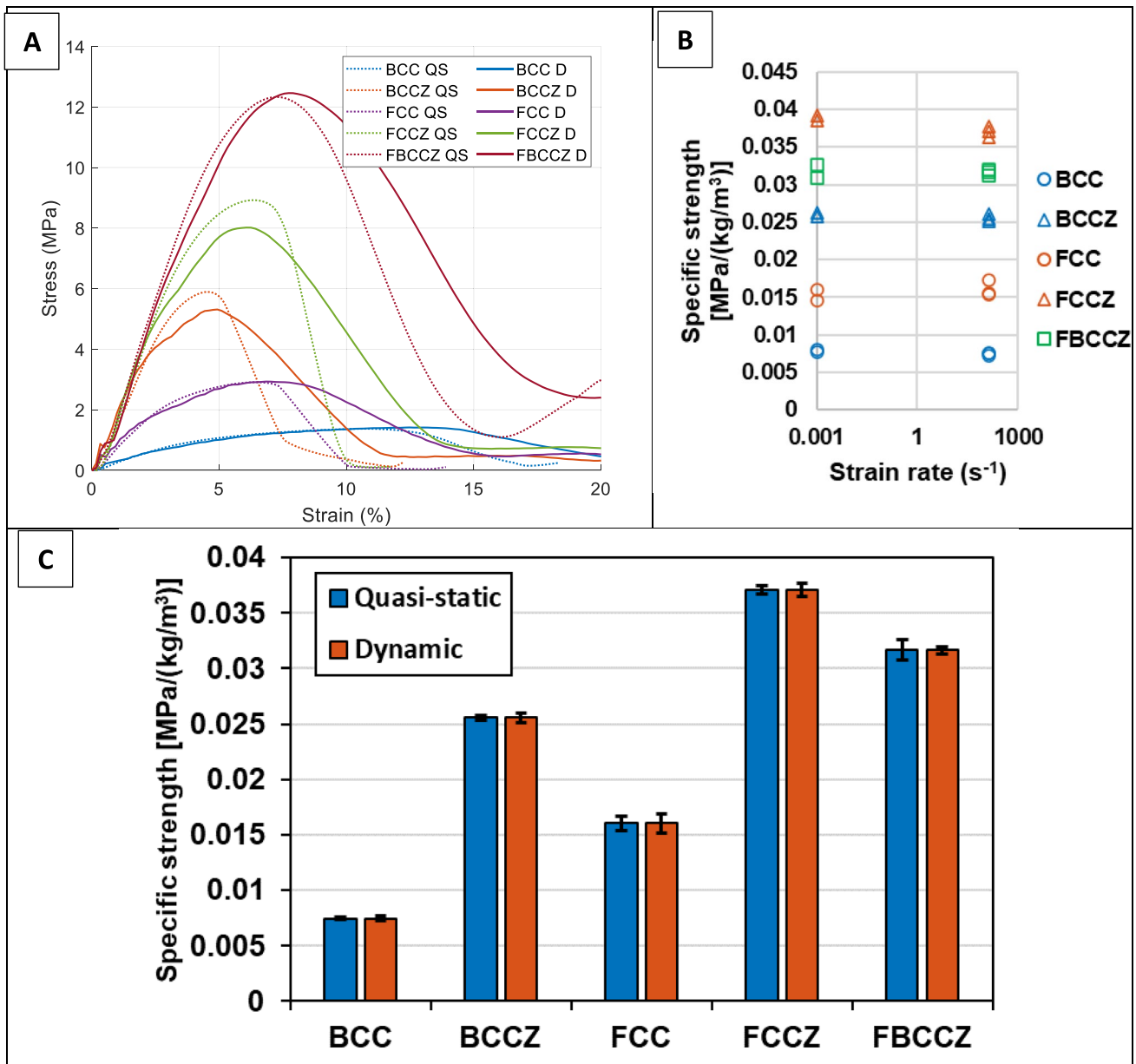


**Fig. 11** Comparison of average quasi-static (QS) and dynamic (D) results, including **A** stress–strain curves, **B** specific strength of all specimens over the range of tested strain rates and **C** specific strength of all specimens, error bars indicate one standard deviation

into the deformation modes observed during experiments, rather than accurate prediction of mechanical properties, and thus, despite quantitative variation between numerical and simulated results, the numerical models were considered to be useful for their intended purpose.

The Von Mises stress contours for static and dynamic explicit simulations are compared in Fig. 15, which provide insight into the macroscopic behaviour observed in experiments. The stress contours of the BCC and FCC lattice structures elucidate why shear planes emerge with different orientations depending on the topology. The BCC specimens

show that the struts connecting the diagonally opposite corners carry significantly greater stress than other struts within the lattice, and when diagonal shear planes emerge upon failure, they align with these most loaded struts. Similarly with the FCC specimens, it can be seen that stress is more concentrated in the struts connecting opposite corners, though for FCC these most loaded struts span the faces of the lattice structure, rather than across the whole structure, as seen in the BCC specimens. This again explains the orientation of the shear plane formation in FCC lattice structures, as the struts that carry the greatest loads diagonally span the

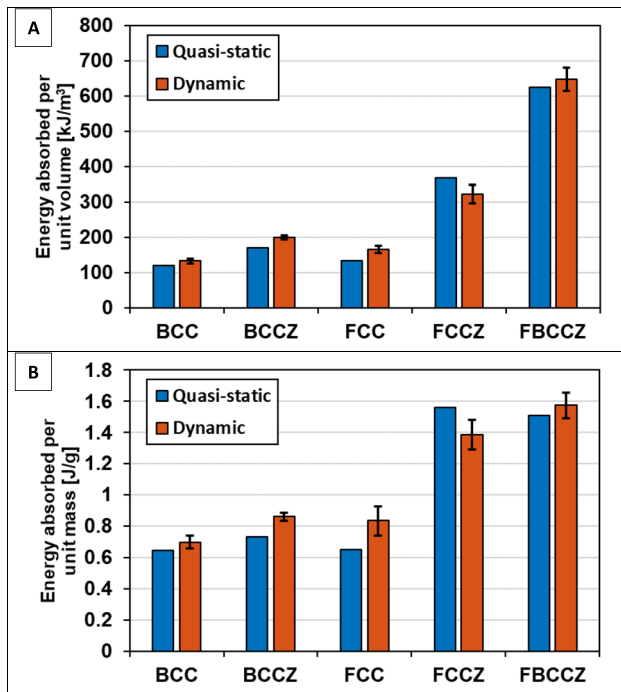


**Fig. 12** Comparison of average quasi-static and dynamic **A** energy absorbed per unit volume and **B** per unit mass

outfaces of the FCC lattice structure, and when shear planes emerge, they align with these most loaded struts.

It is also apparent from the stress contours of the BCC and FCC topologies that stress is greatest in struts furthest from the central  $z$ -axis of the specimens, suggesting that bending moments are induced within the lattice structures during deformation, and as the moment arm increases in length the further from the centre of the lattice, the struts on the outer faces carry the greatest stress. At a certain load, these induced stresses exceed the strength of the struts, leading to the emergence of diagonal shear planes oriented in alignment with the most loaded struts, resulting in failure. In comparison, the BCCZ and FCCZ specimens both show that when  $z$ -struts are included in these topologies these struts carry the greatest stress. This is to be expected, as the  $z$ -struts are aligned to the load meaning that they fail by crushing or buckling, whereas the BCC or FCC struts deform by bending, and so require lower stresses for deformation.

Stress contours also show that stresses are most concentrated in the interfacial layers between the compression plates and the lattice structures. This is consistent with the deformation behaviour observed during experiments, as presented in Figs. 5 and 9, where the deformation of  $z$ -struts in the upper and lower layers is most significant. This effect is more pronounced in the dynamic explicit simulations, suggesting that the concentration of stress in the interfacial

layers increases with dynamic loading. This phenomenon is commonly observed in dynamically loaded materials and is related to stress wave propagation—as Lu states “high stress brought about by the strong plastic compression waves may cause local plastic collapse” [60]. It is likely these effects would be more pronounced at greater strain rates [61] and suggest specimens with  $z$ -struts may be more susceptible to wave effects, though this is not clearly apparent in the tested strain rate range.

The greater concentration of stress in the impacted layer of cells helps explain the formation of shear planes in specimens with  $z$ -struts. For these lattice structures to deform, the  $z$ -struts must collapse by either buckling or crushing (depending on their slenderness), and the struts in the interfacial layers see the greatest stresses due to direct contact with the compression plates. Once these  $z$ -struts fail, the struts connecting diagonally opposite corners take up the loads, leading to the subsequent concentration of stress in these diagonal struts. Shear planes then emerge aligned to these most loaded struts, as observed in the specimens absent of  $z$ -struts.

The stress distributions also help explain the differences in efficiency between the different lattice topologies, quantified by specific strength and energy absorption. The BCC, FCC and BCCZ topologies were found to have the lowest specific strength and energy absorption capabilities, and the reason for this is demonstrated by the significant variation in stress states of the individual lattice struts through the structures. This is particularly pronounced for the BCC and BCCZ stress contours presented in Fig. 15, as there is significant variation in stress values between the different struts. As few struts are carrying significant stresses, while most struts are barely stressed at all, this leads to inefficiency of the structure, as much of the material present is underutilised, and is observed as reduced specific strength and energy absorption efficiency in experiments. The FCCZ topology had the most even distribution of stress amongst its constituent struts, and so was the most efficient by these measures.

The FBCCZ topology can be considered a hybrid of the other tested topologies as it includes BCC, FCC and  $z$ -struts. Similar phenomena are observed during early deformation of this topology compared to the others—stress is most concentrated in the  $z$ -struts and increases further away from the central  $z$ -axis and in the upper and lower layers. However, once these struts fail, there are both FCC and BCC struts present to take up loads; no single plane emerges across which stresses are greatest, and so no clear shear planes emerge upon failure. Rather, the FBCCZ specimens failed in an inconsistent manner and more progressively, seen in the deformation images in Figs. 5 and 9 and the stress–strain curves in Fig. 11A. As a result, FBCCZ specimens had the greatest strength and stiffness, and failed more progressively

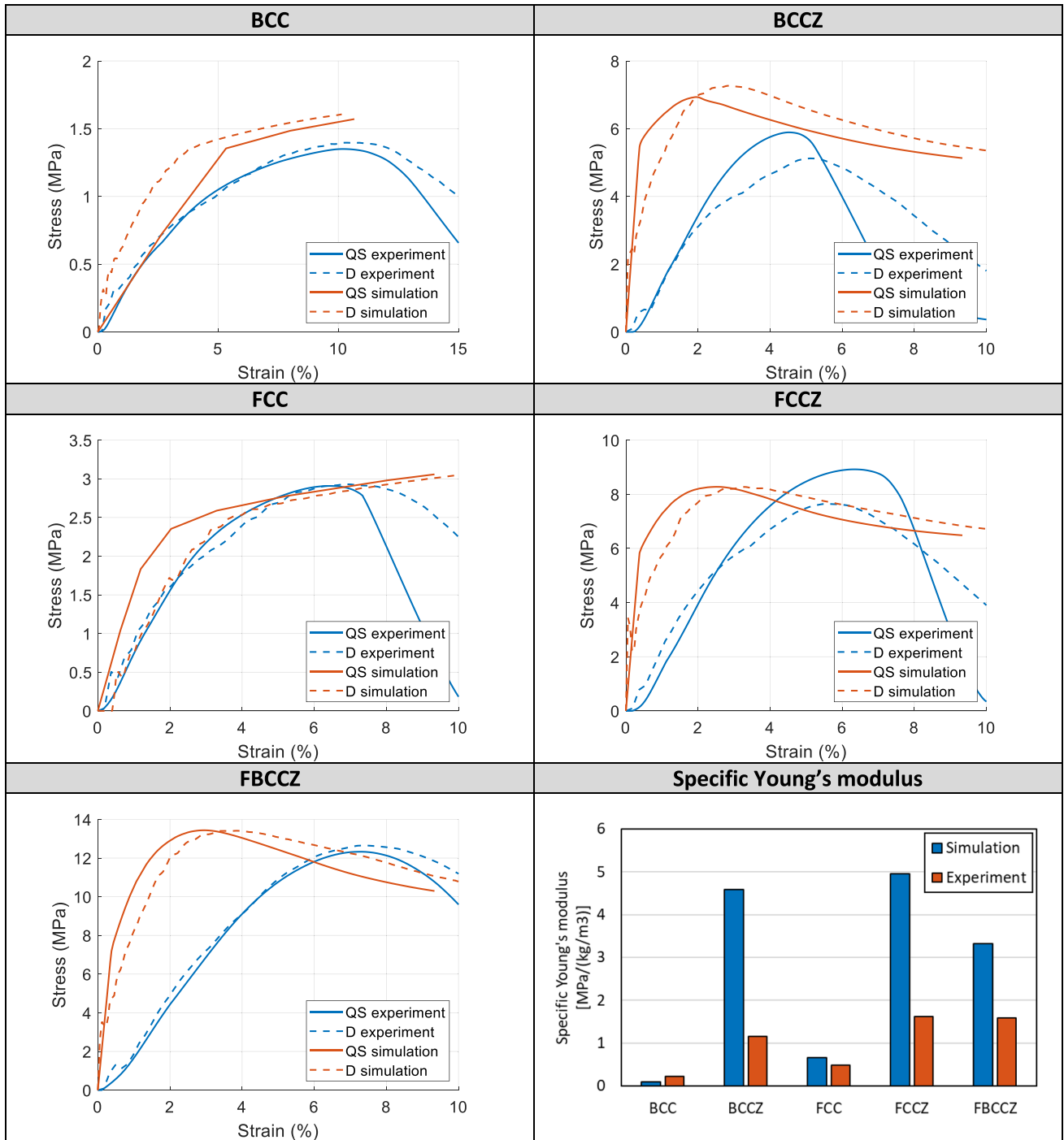


**Fig. 13** Comparison of quasi-static (QS) and dynamic (D) stress–strain curves and specific Young’s modulus between simulations and experiments for all topologies



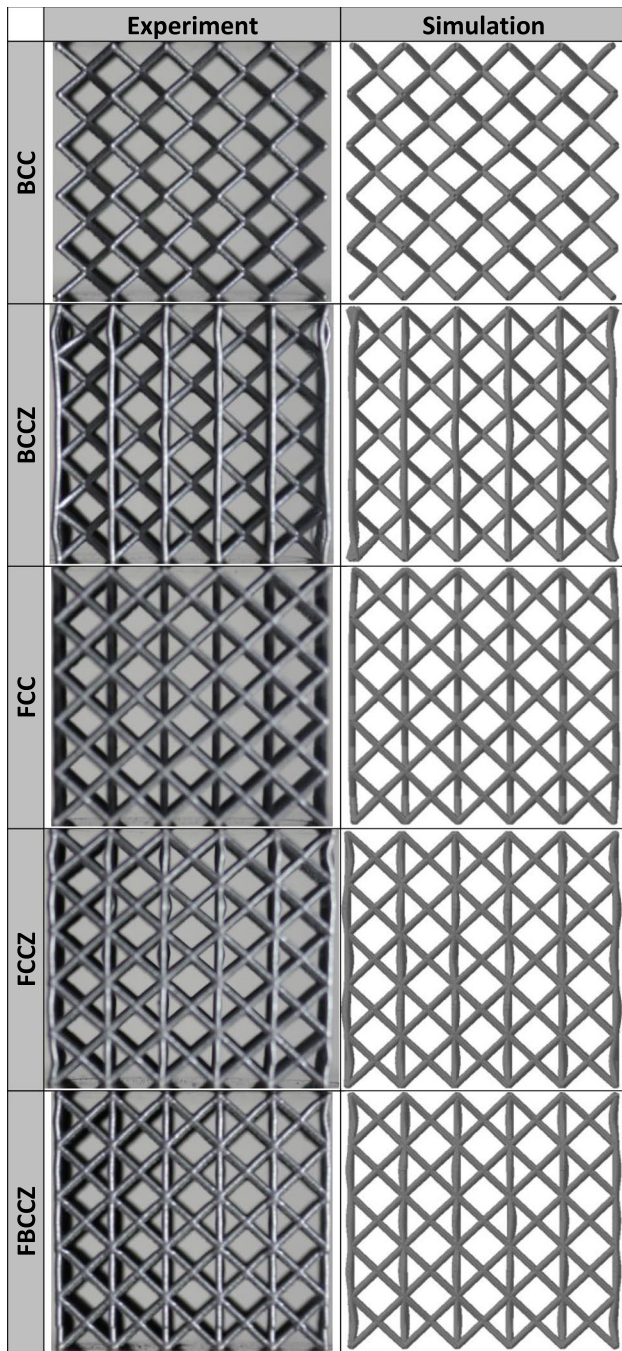


**Fig. 14** Comparison of experimental and simulation deformation behaviour of all topologies

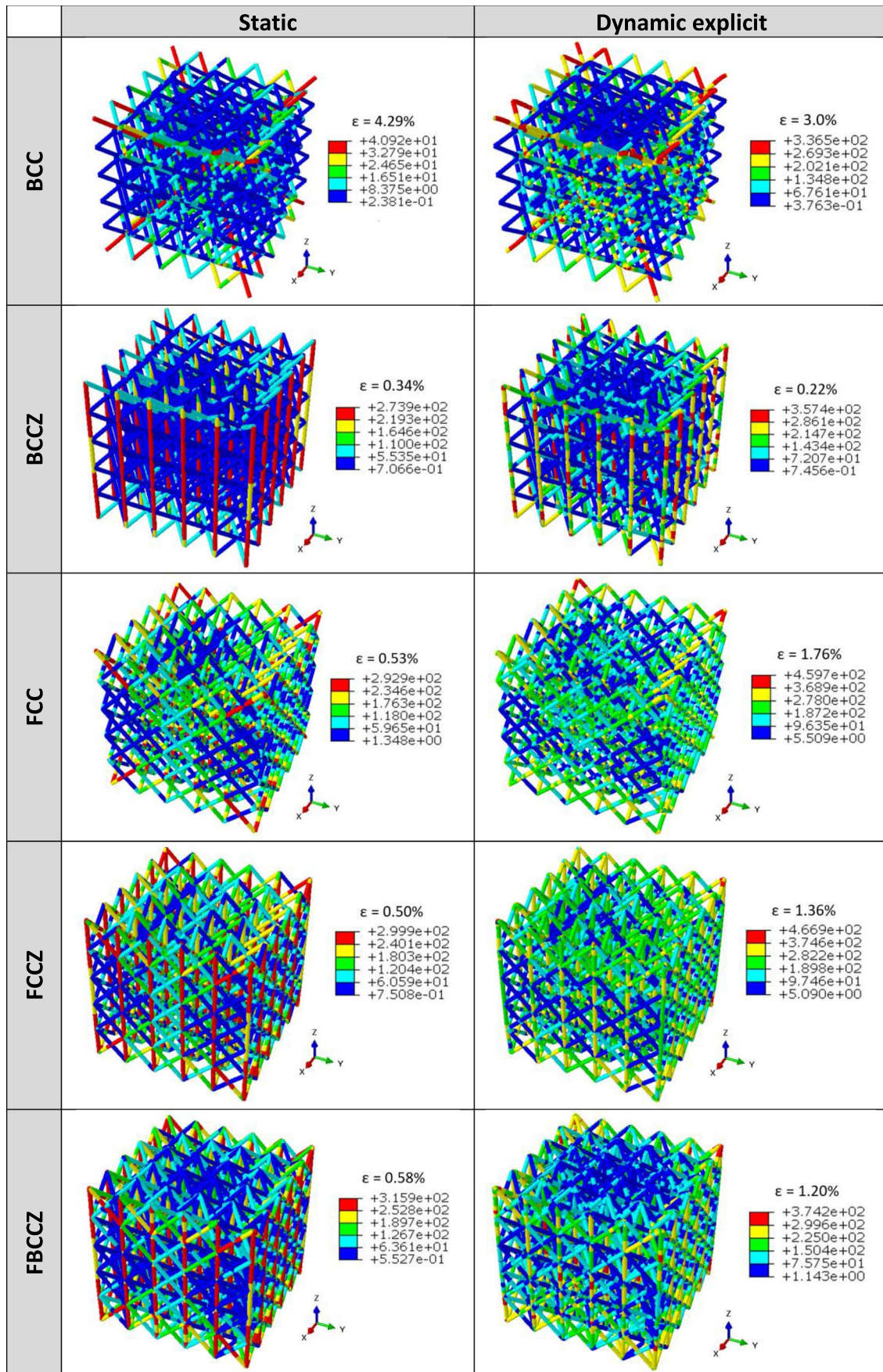
than other topologies, but were less predictable in their failure, the reasons for which can be inferred from the stress contours of the numerical model.

## 6 Concluding remarks

Despite the research attention AM lattice structures have recently received, mechanical characterisation of the dynamic performance of AlSi10Mg lattice structures remains relatively undefined. This research has sought to overcome this identified deficit by investigating the effects of topology on the dynamic behaviour of SLM AlSi10Mg lattice structures. The findings of this research contribute to this characterisation and provide a foundation for further research on the broader dynamic behaviour of AM lattice structures.

The key findings of this work are:

- The as-manufactured relative density of BCC, BCCZ and FBCCZ specimens was found to exceed the expected value, whereas CAD relative densities of FCC and FCCZ topologies were found to underpredict the as-manufactured relative density. This is due to the different build orientations of their constituent struts, which affects their fidelity of as-manufactured geometries, and the different arrangements of struts and whether struts are shared between cells, which is dependent on topology.
- The inclusion of z-struts in BCC and FCC specimens led to an increase in strength and stiffness, but a reduction in compliance, which was consistent for both quasi-static and dynamic testing.
- The FCCZ topology was found to be the most efficient topology in terms of specific strength and energy absorption, due to the more even distribution of stresses across the structure during deformation.
- Specimens failed by the emergence of diagonal shear planes, the orientation of which is dependent on topology, but increasing strain rate did not alter this failure mechanism. The reason for the orientation of these shear planes was demonstrated by the numerical models that showed that stress is concentrated in struts connecting diagonally opposite corners of the structure, and when shear planes emerge, they are aligned to these most loaded struts.
- Unloading modulus increased with the strain at which it was measured and was consistently greater than the Young's modulus for all topologies.
- Stress–strain behaviour was largely consistent across the tested strain rate range for all topologies, although deformation generally occurred at greater strains under dynamic loading due to the greater rate of deformation during dynamic testing.
- Although some variation in specific strength was noticed between quasi-static and dynamic results, mean values were very similar, suggesting there is no significant rate sensitivity of the tested lattice structures



◀ **Fig. 15** Von Mises stress distribution (MPa) in static and dynamic explicit numerical models of lattice for all topologies

in the range of strain rates tested. However, some limited wave effects were observed in numerical models, suggesting rate sensitivity effects could be greater at greater strain rates.

- The accuracy of numerical models was found to vary depending on topology, with the stiffness of simulations of lattice structures including z-struts consistently exceeding the experimentally observed stiffness, due the sensitivity of their mechanical response to the orientation of loads. However, qualitative behaviour was found to be consistent with experimentally observed behaviour, and the models provide insight into the deformation modes observed during experimental testing. Specifically, the concentration of stress in specific struts and the implications for the emergence of shear planes, and the distribution of stress across the structure elucidate the causes of failure and the macroscopically observed efficiency of the tested lattice topologies.

**Acknowledgements** The authors would like to acknowledge the financial support from the members of the ARC Training Centre for Lightweight Automotive Structures and from the Australian Research Council (Grant Reference IC160100032), the scientific and technical assistance of the Swinburne University of Technology Impact Engineering Laboratory and the scientific and technical assistance of the RMIT Advanced Manufacturing Precinct.

**Author contribution** Tobias Maconachie: conceptualization; methodology; software; formal analysis; investigation; data curation; writing—original draft; writing—review and editing; visualisation.

Martin Leary: conceptualization; methodology; writing—original draft; writing—review and editing; supervision; project administration; funding acquisition.

Phuong Tran: writing—review and editing; supervision.

Jonathan Harris: writing—review and editing; supervision.

Qiang Liu: writing—review and editing.

Guoxing Lu: resources, project administration, funding acquisition.

Dong Ruan: resources; writing—review and editing; supervision.

Omar Faruque: resources, supervision, project administration, funding acquisition.

Milan Brandt: resources, supervision, project administration, funding acquisition.

**Funding** Funding for this project was provided by the ARC Training Centre for Lightweight Automotive Structures (ATLAS), Australian Research Council Grant IC160100032.

**Availability of data and material** The raw/processed data required to reproduce these findings cannot be shared at this time as the data also forms part of an ongoing study.

**Code availability** The code required to reproduce these findings cannot be shared at this time as the data also forms part of an ongoing study.

## Declarations

**Ethics approval** Not applicable.

**Consent to participate** Not applicable.

**Consent for publication** Not applicable.

**Competing interests** The authors declare no competing interests.

## References

1. Ahuja B, Karg M, Schmidt M (2015) Additive manufacturing in production: challenges and opportunities. International Society for Optics and Photonics
2. Yan C et al (2014) Evaluation of light-weight AlSi10Mg periodic cellular lattice structures fabricated via direct metal laser sintering. *J Mater Process Technol* 214(4):856–864
3. Gibson LJ, Ashby MF (1997) Cellular solids: structure and properties. Cambridge University Press, Cambridge
4. Murr LE et al (1917) Next-generation biomedical implants using additive manufacturing of complex, cellular and functional mesh arrays. *Philos Trans R Soc A Math Phys Eng Sci* 2010(368):1999–2032
5. Hao Z et al (2018) Lightweight structure of a phase-change thermal controller based on lattice cells manufactured by SLM. *Chin J Aeronaut*
6. Wang Y et al (2018) Design of graded lattice structure with optimized mesostructures for additive manufacturing. *Mater Des* 142:114–123
7. Yavari SA et al (2015) Relationship between unit cell type and porosity and the fatigue behavior of selective laser melted meta-biomaterials. *J Mech Behav Biomed Mater* 43:91–100
8. Leary M et al (2018) Inconel 625 lattice structures manufactured by selective laser melting (SLM): mechanical properties, deformation and failure modes. *Mater Des* 157:179–199
9. Xiong J et al (2015) Advanced micro-lattice materials. *Adv Eng Mater* 17(9):1253–1264
10. Mazur M et al (2017) 5 - Mechanical properties of Ti6Al4V and AlSi12Mg lattice structures manufactured by selective laser melting (SLM). In: Brandt M (ed) *Laser Additive Manufacturing*. Woodhead Publishing, pp 119–161
11. Schaedler TA et al (2011) Ultralight metallic microlattices. *Science* 334(6058):962–965
12. Hao L et al. Design and additive manufacturing of cellular lattice structures
13. Liu C et al (2017) Additive manufacturing-oriented design of graded lattice structures through explicit topology optimization. *J Appl Mech* 84(8):081008
14. Ashby MF, Medalist RM (1983) The mechanical properties of cellular solids. *J Mater Sci* 14(9):1755–1769
15. Yan C et al (2012) Evaluations of cellular lattice structures manufactured using selective laser melting. *Int J Mach Tools Manuf* 62:32–38
16. Leary M et al (2016) Selective laser melting (SLM) of AlSi12Mg lattice structures. *Mater Des* 98:344–357
17. Koehnen P et al (2018) Mechanical properties and deformation behavior of additively manufactured lattice structures of stainless steel. *Mater Des* 145:205–217
18. Yavari SA et al (2013) Fatigue behavior of porous biomaterials manufactured using selective laser melting. *Mater Sci Eng C* 33(8):4849–4858

19. Harris JA, Winter RE, McShane GJ (2017) Impact response of additively manufactured metallic hybrid lattice materials. *Int J Impact Eng* 104:177–191
20. Smith M et al (2010) The quasi-static and blast response of steel lattice structures. *J Sandwich Struct Mater* 13(4):479–501
21. McKown S et al (2008) The quasi-static and blast loading response of lattice structures. *Int J Impact Eng* 35(8):795–810
22. Tancogne-Dejean T, Spierings AB, Mohr D (2016) Additively-manufactured metallic micro-lattice materials for high specific energy absorption under static and dynamic loading. *Acta Mater* 116:14–28
23. Ruan D et al (2002) Compressive behaviour of aluminium foams at low and medium strain rates. *Compos Struct* 57(1):331–336
24. Maconachie T et al (2019) SLM lattice structures: properties, performance, applications and challenges. *Mater Des* 108137
25. Ashby M (1838) The properties of foams and lattices. *Philos Trans R Soc A Math Phys Eng Sci* 2005(364):15–30
26. Deshpande VS, Ashby MF, Fleck NA (2001) Foam topology: bending versus stretching dominated architectures. *Acta Mater* 49(6):1035–1040
27. Ashby MF (2005) Hybrids to fill holes in material property space. *Phil Mag* 85(26–27):3235–3257
28. Brandt M (2016) *Laser additive manufacturing: materials, design, technologies, and applications*. Woodhead Publishing
29. Chen W et al (2019) Stiff isotropic lattices beyond the Maxwell criterion. *Science Adv* 5(9):eaaw1937
30. Mazur M et al (2016) Deformation and failure behaviour of Ti-6Al-4V lattice structures manufactured by selective laser melting (SLM). *Int J Adv Manuf Technol* 84(5):1391–1411
31. Gusarov AV, Kruth JP (2005) Modelling of radiation transfer in metallic powders at laser treatment. *Int J Heat Mass Transf* 48(16):3423–3434
32. Maconachie T et al (2020) Effect of build orientation on the quasi-static and dynamic response of SLM AlSi10Mg. *Mater Sci Eng A* 788:139445
33. Leary M et al (2019) Mechanical and thermal characterisation of AlSi10Mg SLM block support structures. *Mater Des* 183:108138
34. Ashby MF et al (2000) *Metal foams: a design guide*. Elsevier
35. Luxner MH, Stampfl J, Pettermann HE (2005) Finite element modeling concepts and linear analyses of 3D regular open cell structures. *J Mater Sci* 40(22):5859–5866
36. Smith M, Guan Z, Cantwell W (2013) Finite element modelling of the compressive response of lattice structures manufactured using the selective laser melting technique. *Int J Mech Sci* 67:28–41
37. Labeas GN, Sunaric MM (2010) Investigation on the static response and failure process of metallic open lattice cellular structures. *Strain* 46(2):195–204
38. Lei H et al (2019) Evaluation of compressive properties of SLM-fabricated multi-layer lattice structures by experimental test and  $\mu$ -CT-based finite element analysis. *Mater Des* 169:107685
39. Guo H et al (2020) Finite element simulation of the compressive response of additively manufactured lattice structures with large diameters. *Comput Mater Sci* 175:109610
40. de Galarreta SR, Jeffers JR, Ghouse S (2020) A validated finite element analysis procedure for porous structures. *Mater Des* 189:108546
41. Cao X et al (2020) Compression experiment and numerical evaluation on mechanical responses of the lattice structures with stochastic geometric defects originated from additive-manufacturing. *Compos B Eng* 194:108030
42. Rosenthal I, Stern A, Frage N (2017) Strain rate sensitivity and fracture mechanism of AlSi10Mg parts produced by selective laser melting. *Mater Sci Eng A* 682:509–517
43. Nurel B et al (2018) Split Hopkinson pressure bar tests for investigating dynamic properties of additively manufactured AlSi10Mg alloy by selective laser melting. *Addit Manuf* 22:823–833
44. Al-Rubaie KS et al (2020) Machinability of SLM-produced Ti6Al4V titanium alloy parts. *J Manuf Process* 57:768–786
45. Uzan NE et al (2018) On the effect of shot-peening on fatigue resistance of AlSi10Mg specimens fabricated by additive manufacturing using selective laser melting (AM-SLM). *Addit Manuf* 21:458–464
46. Aboulkhair NT et al (2014) Reducing porosity in AlSi10Mg parts processed by selective laser melting. *Addit Manuf* 1–4:77–86
47. Li W et al (2016) Effect of heat treatment on AlSi10Mg alloy fabricated by selective laser melting: microstructure evolution, mechanical properties and fracture mechanism. *Mater Sci Eng A* 663:116–125
48. Aboulkhair NT et al (2016) The microstructure and mechanical properties of selectively laser melted AlSi10Mg: the effect of a conventional T6-like heat treatment. *Mater Sci Eng A* 667:139–146
49. Maconachie T et al (2020) Effect of build orientation on the quasi-static and dynamic response of SLM AlSi10Mg. *Mater Sci Eng A* 139445
50. Giovagnoli M et al (2021) Effect of different heat-treatment routes on the impact properties of an additively manufactured AlSi10Mg alloy. *Mater Sci Eng A* 802:140671
51. Tridello A et al (2019) VHCF response of Gaussian SLM AlSi10Mg specimens: effect of a stress relief heat treatment. *Int J Fatigue* 124:435–443
52. Sufiiarov V et al (2020) Investigation of accuracy, microstructure and properties of additive manufactured lattice structures. *Mater Today Proc* 30:572–577
53. Hazeli K et al (2019) Microstructure-topology relationship effects on the quasi-static and dynamic behavior of additively manufactured lattice structures. *Mater Des* 176:107826
54. Jin Y, Qin SJ, Huang Q (2015) Out-of-plane geometric error prediction for additive manufacturing. in 2015 IEEE International Conference on Automation Science and Engineering (CASE). IEEE
55. Leary M (2017) Surface roughness optimisation for selective laser melting (SLM): accommodating relevant and irrelevant surfaces. *Laser additive manufacturing*. Elsevier, pp 99–118
56. Alghamdi A et al (2020) Effect of additive manufactured lattice defects on mechanical properties: an automated method for the enhancement of lattice geometry. *Int J Adv Manuf Technol* 108:957–971
57. Alghamdi A et al (2021) Buckling phenomena in am lattice strut elements: a design tool applied to Ti-6AL4V Lb-Pbf. *Mater Des* 109892
58. Yang L (2015) Experimental-assisted design development for an octahedral cellular structure using additive manufacturing. *Rapid Prototyp J*
59. Leary M et al (2021) 7 - Surface roughness. In: Yadroitsev I et al (eds) *fundamentals of laser powder bed fusion of metals*. Elsevier, pp 179–213
60. Lu G, Yu TX (2003) Energy absorption of structures and materials. Elsevier
61. Deshpande VS, Fleck NA (2000) High strain rate compressive behaviour of aluminium alloy foams. *Int J Impact Eng* 24(3):277–298

**Publisher's note** Springer Nature remains neutral with regard to jurisdictional claims in published maps and institutional affiliations.